Supplementary Materials

Atomic-scale insights into halide perovskite device degradation via multidimensional *in situ* electron microscopy

Xinjuan Li[1], Qichun Gu[2], Wei Huang[1], Simon M. Fairclough[1], Richard H. Friend[3], Samuel D. Stranks[2,3], Tianjun Liu[3]*, Caterina Ducati[1]*

Affiliations:

[1] Department of Materials Science and Metallurgy, University of Cambridge, Cambridge CB3 0FS, UK

[2] Department of Chemical Engineering and Biotechnology, University of Cambridge, Philippa Fawcett Drive, Cambridge CB3 0AS, UK

[3] Cavendish Laboratory, University of Cambridge, JJ Thomson Avenue, Cambridge CB3 0HE, UK

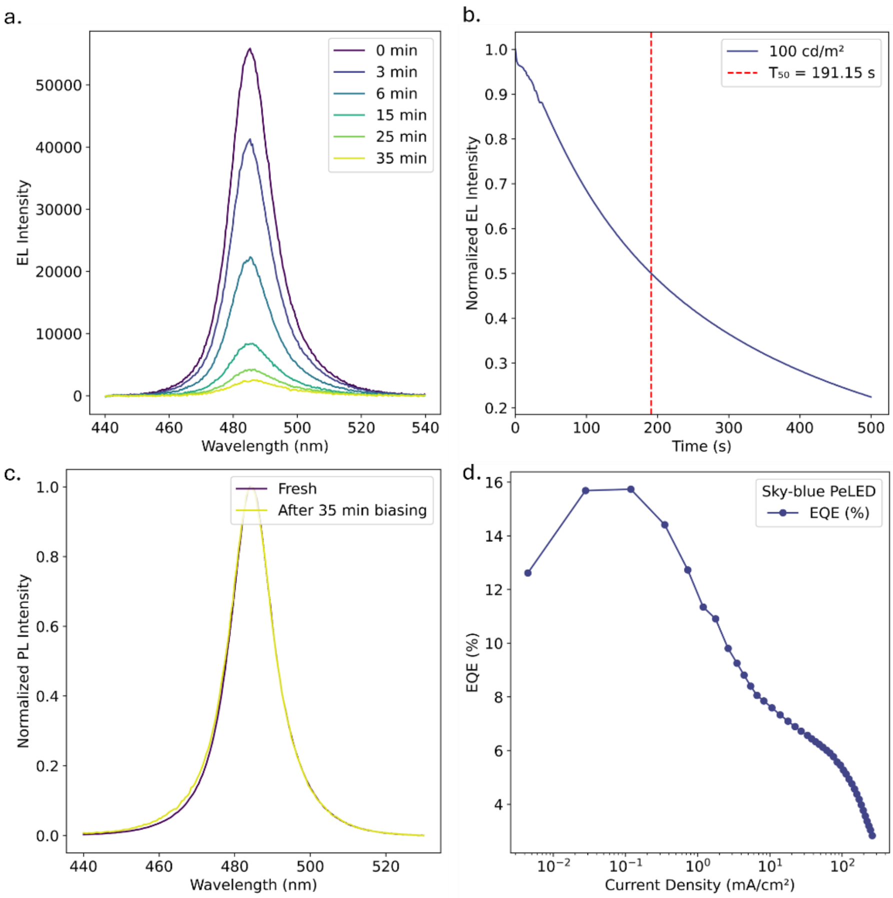

Supplementary Fig. 1 | The optoelectronic characterization of a $CsPb(Br_{0.65}Cl_{0.35})_3$ blue perovskite LED under electrical biasing. a, Time-resolved electroluminescence (EL) spectra collected at 0, 3, 6, 15, 25, 35 mins during continuous device operation, revealing progressive spectral evolution under bias. b, EL stability plot showing the T_{50} of a sky-blue emitting device under constant current driving conditions. c, Photoluminescence (PL) spectra of the fresh device and after 35 mins of electrical stress, illustrating degradation in emission intensity. D. The EQE of the PeLED.

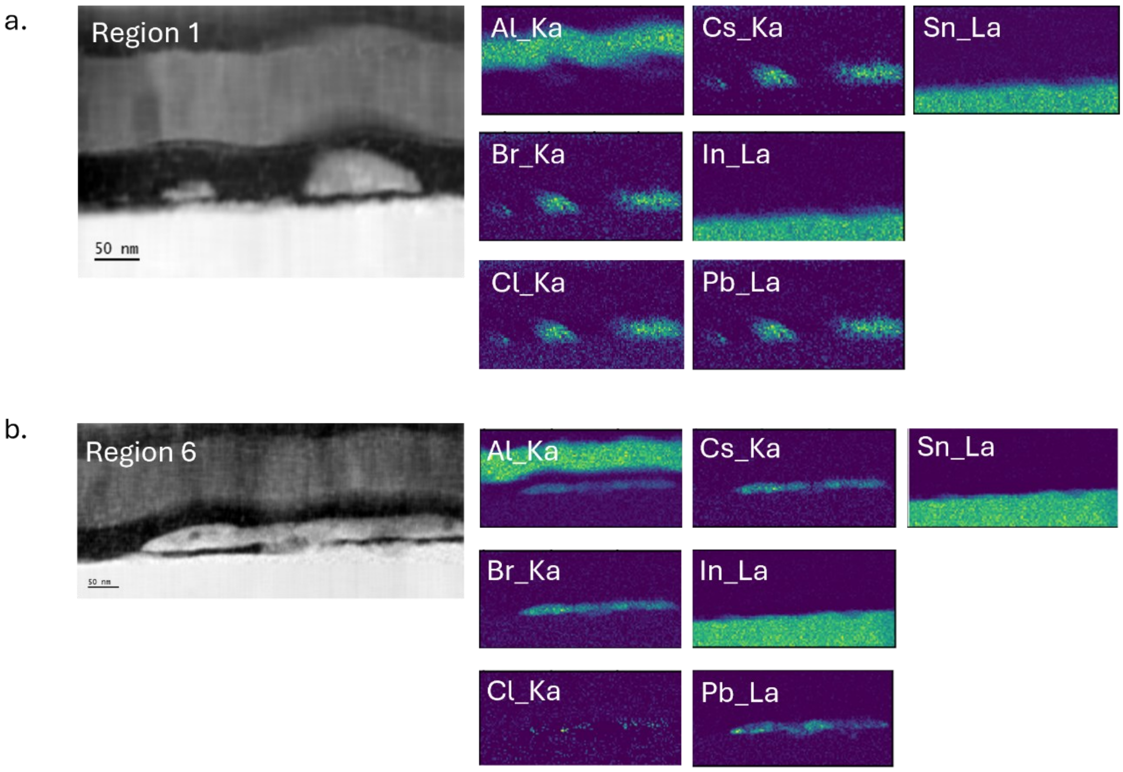

Supplementary Fig. 2 | STEM-EDX elemental mapping of the blue perovskite nanoLED before and after electrical biasing. Elemental distributions are shown for region 1 (a) in the pristine device and Region 6 (b) after 35 minutes of electrical biasing. Comparative analysis reveals changes in elemental uniformity and possible ion migration, or phase segregation associated with electrical stress.

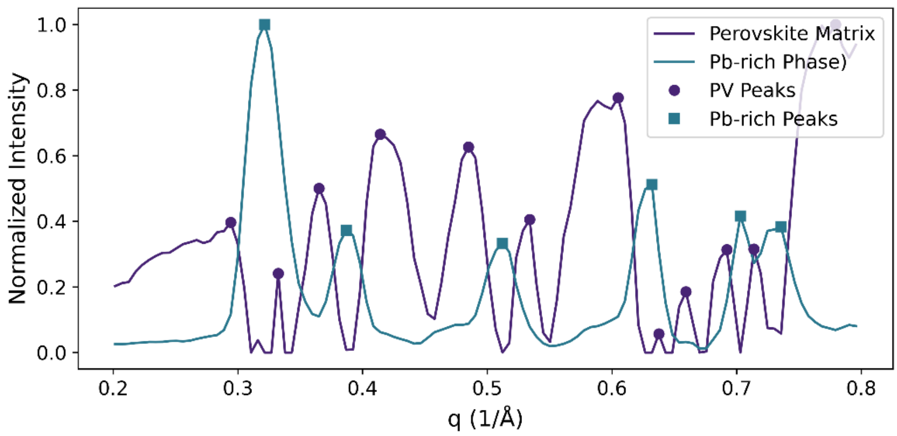

Supplementary Fig. 3 | NMF-decomposed 1D radial electron diffraction patterns revealing phase separation in biased perovskite nanoLED from region 6 after 35 minutes of electrical biasing, separating the signal from the primary perovskite emitter and the degraded Pb-rich phases, highlighting phase segregation induced by prolonged electrical stress.

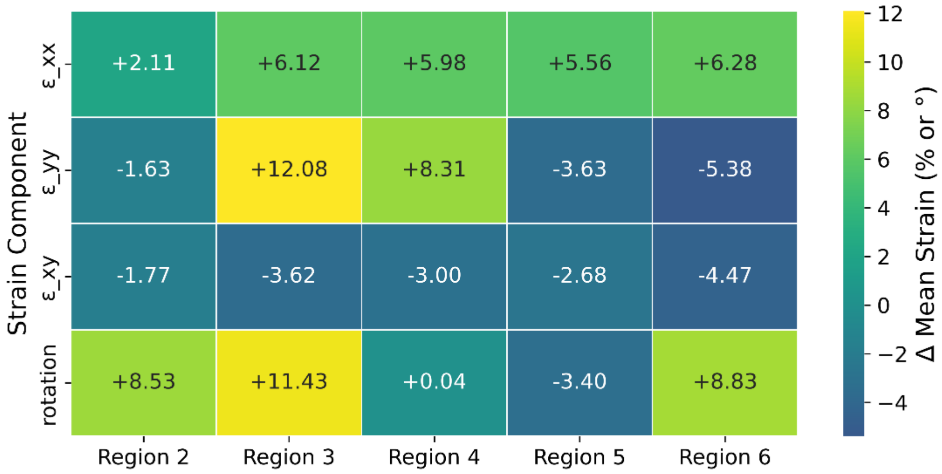

Supplementary Fig. 4 | Relative strain tensor evolution in the perovskite nanoLED under electrical biasing. Different strain components—εxx, εyy, εxy, and in-plane rotation (θ), shown as the change relative to region 1 (pristine reference).

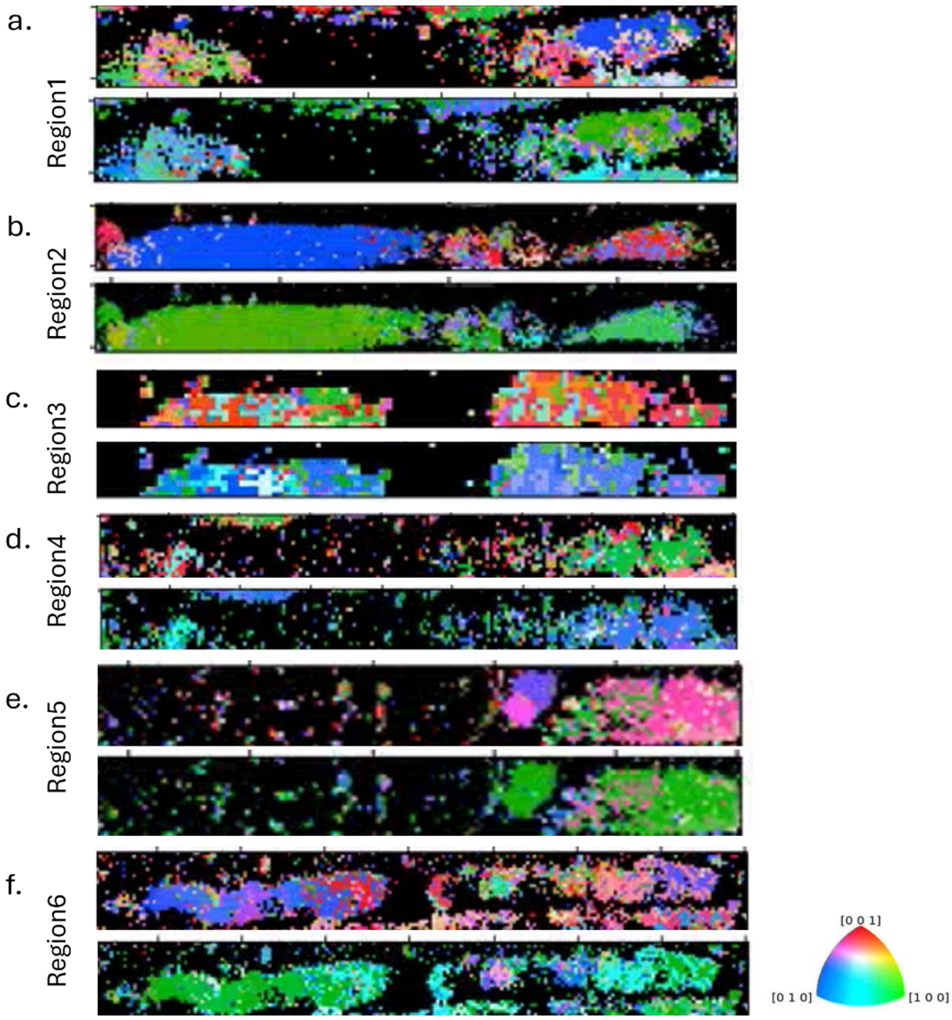

Supplementary Fig. 5 | Crystallographic orientation evolution across biased regions in the perovskite nanoLED. In-plane (top) and out-of-plane (bottom) orientation maps extracted from region 1 (pristine) to Region 6 (after 35 minutes of electrical biasing).

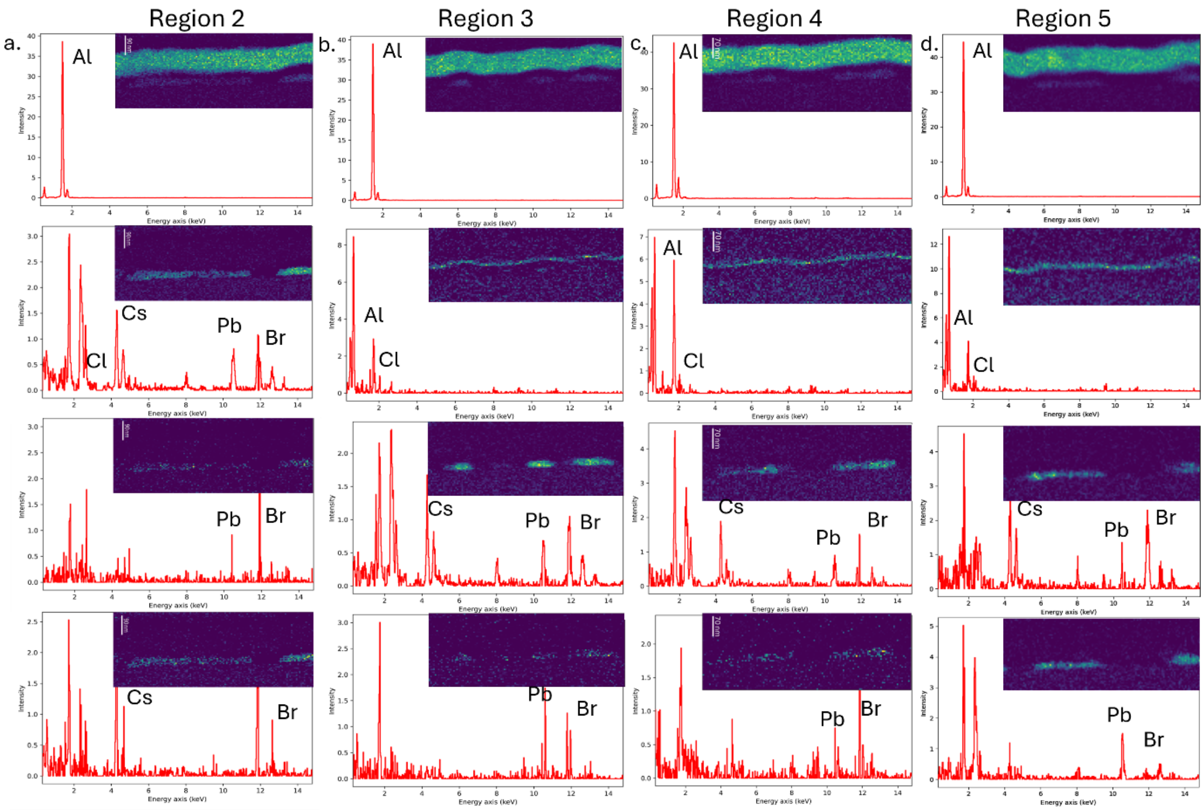

Supplementary Fig. 6 | Multivariate decomposition of STEM–EDX spectra revealing chemical phase evolution under bias. Principal component analysis (PCA) and non-negative matrix factorization (NMF) applied to STEM–EDX spectral datasets from region 2 to 5 of the biased perovskite nanoLED. Distinct spectral components corresponding to the Al cathode, $AlCl_3$-rich degradation byproducts, the primary perovskite emitter, and Pb-rich phases are resolved, illustrating complex chemical transformations during device operation.

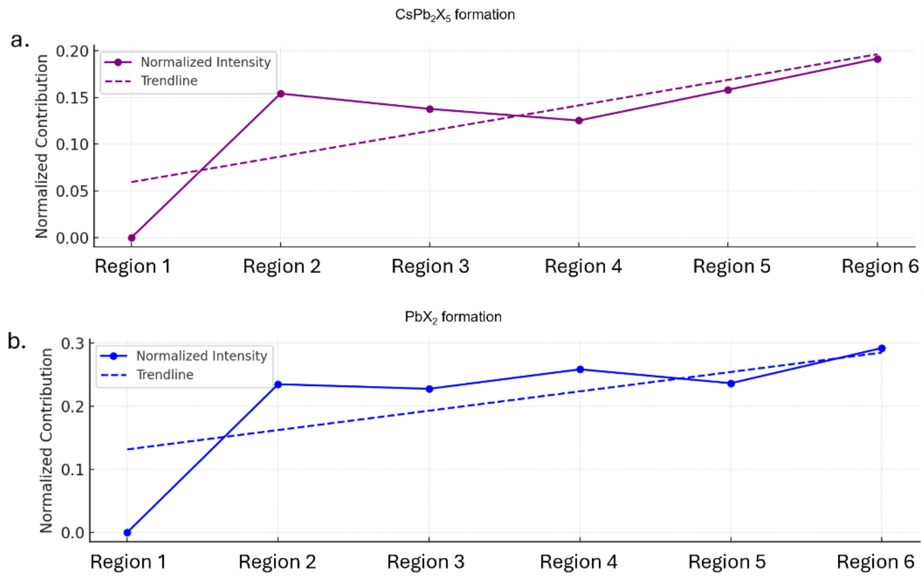

Supplementary Fig. 7 | The normalized intensity integration for Pb-rich phases from 1D radial profiles extracted from SED dataset after polar for region 1 to 6 from pristine to biasing conditions. The trendline has demonstrated the Pb-rich phases' concentration changes with increasing biasing times.

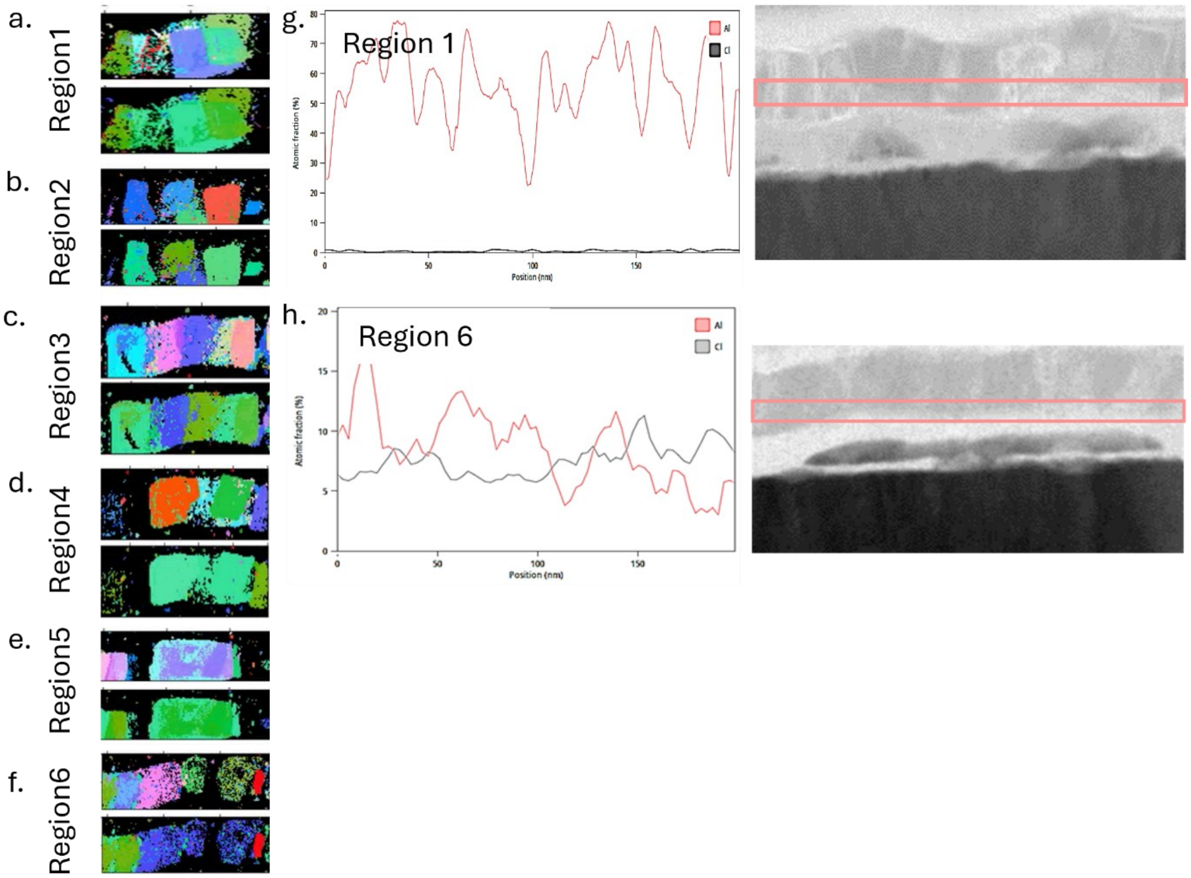

Supplementary Fig. 8 | (a-f) The crystal orientation map in both in-plane (top layer) and out-of-plane direction (bottom layer), of metallic Al cathode area, cropped from main device area with emitter. The orientation maps of metallic cathode with different biasing time are generated with template matching of (Fm3m 225) cubic crystal structure to imply the crystal orientation changes. (g-h) The STEM-EDX line spectrum extracted from highlighted region in vBF images presented, indicating the formation of new composition $AlCl_3$ beneath the Al contact after 35 mins biasing.

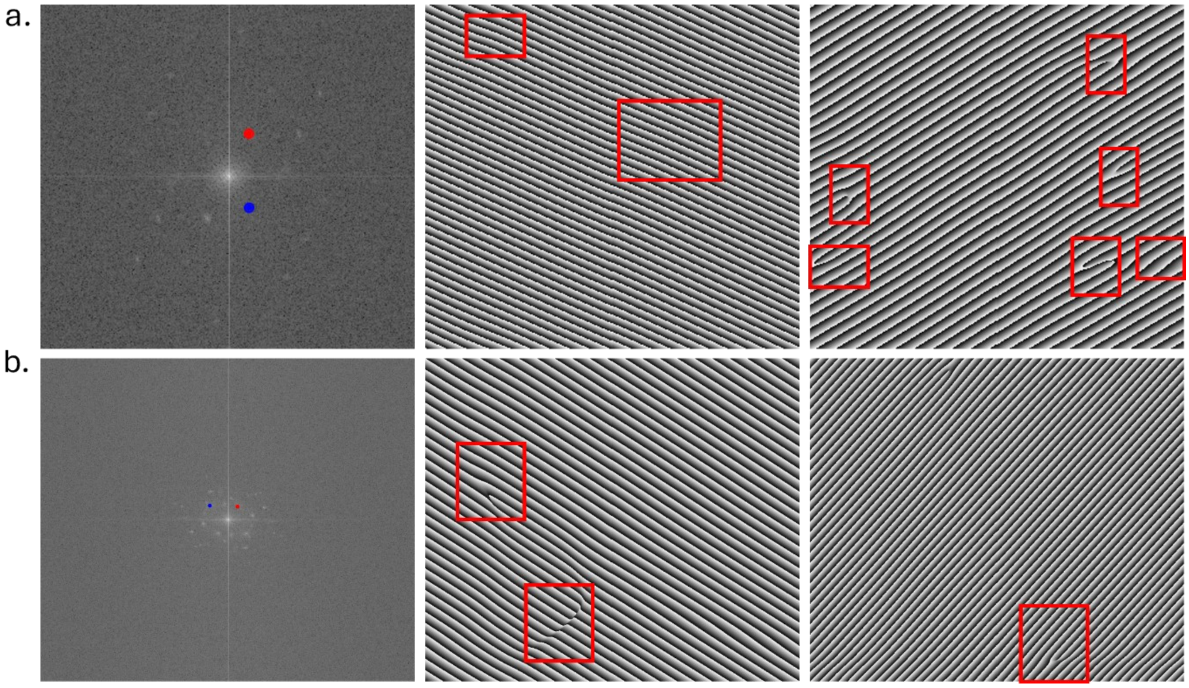

Supplementary. Fig. 9 | The detailed study of quantifying the changes in lattices, shown in the raw phase images in GPA analysis for the region near ETL (a) and region near HTL(b) at pristine. The chosen masks are placed around two non-collinear Bragg spots for GPA analysis, shown in (a) and (b).

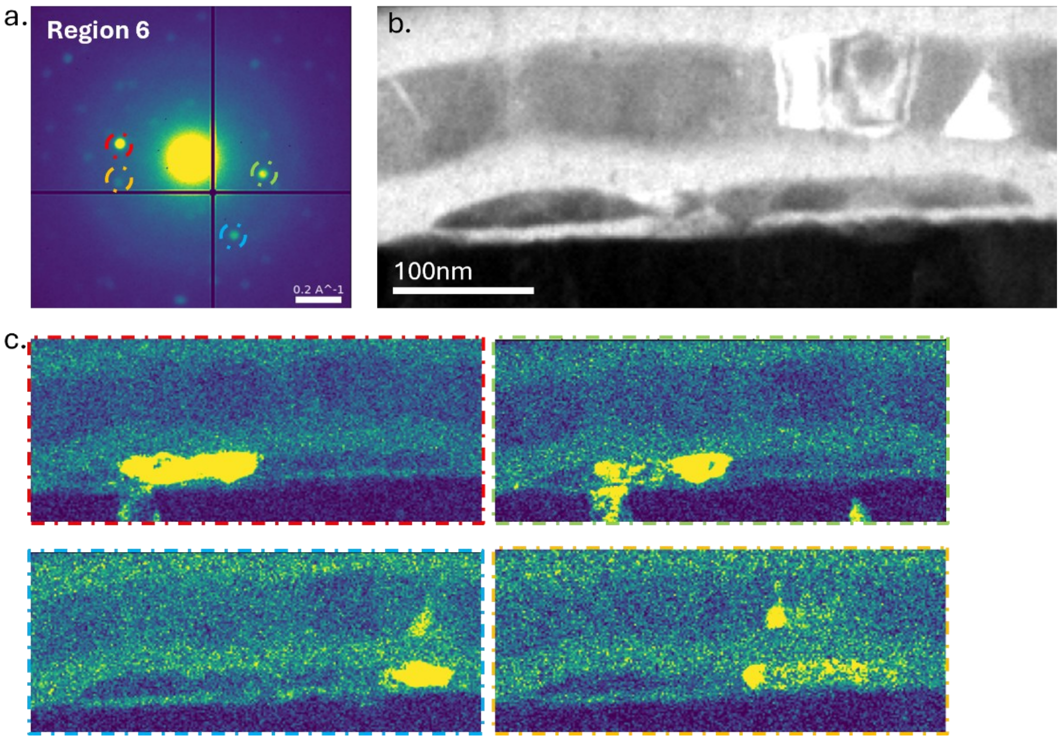

Supplementary Fig. 10 | The mean diffraction patterns in region 6(a, b). (c) The virtual images matched with selected diffraction spots in (a).

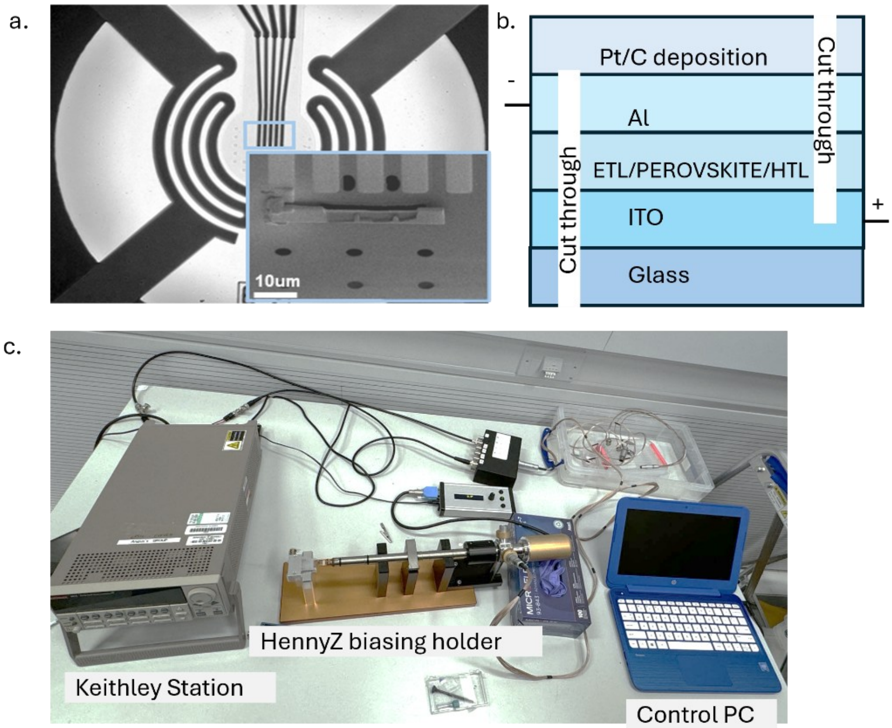

Supplementary. Fig. 11 | The details regarding to operando experimental sets up. (a) A SEM image to illustrate the sample placed on MEMS biasing chip with two electrodes connected. (b) A schematic of designed FIB-lamella sample to make sure it follows the real operation standard. (c) The set up of the HennyZ biasing holder with a Keithley station connected to input a constant current and a control PC to record the given driving voltage during the operation.

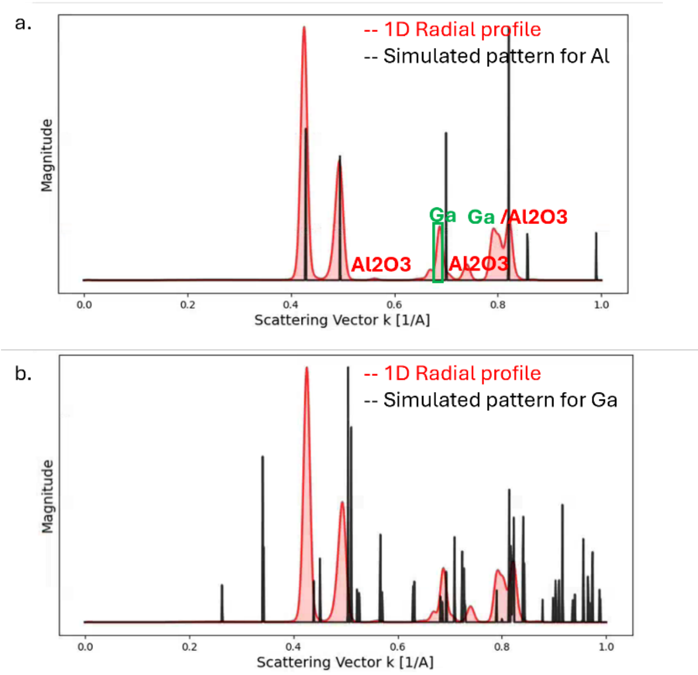

Supplementary. Fig. 12 | The 1D radial diffraction profile of Al contact region before(a) and after(b) biasing with simulated Al pattern. The green box presented in (a) demonstrated the presence of Ga and Al2O3 composition before biasing, owing to the Ga contamination during

Table 1. The lattice parameter extracted for emitters in region 1 to region 6

Condition	a (Å)	±a_err	b (Å)	±b_err	c (Å)	±c_err
Region 1	8.2382	±0.097	11.6224	±0.087	8.2250	±0.064
Region 2	8.5909	±0.190	11.5717	±0.305	7.9614	±0.088
Region 3	8.4571	±0.104	11.8786	±0.114	7.9985	±0.186
Region 4	8.4271	±0.313	11.7889	±0.070	7.9504	±0.054
Region 5	8.6640	±0.139	11.6110	±0.039	8.0708	±0.026
Region 6	8.2054	±0.366	11.8052	±0.246	7.4896	±0.283